Scientific Reports

https://doi.org/10.1038/s41598-026-38393-y

Article in Press

Water geochemistry in the Bozhi-Dabei area, Tarim Basin and its implications for natural gas accumulation in deep basin

Received: 3 July 2025

Accepted: 29 January 2026

Published online: 25 February 2026

Cite this article as: Chen J., Fan Y., Jia W. *et al.* Water geochemistry in the Bozhi-Dabei area, Tarim Basin and its implications for natural gas accumulation in deep basin. *Sci Rep* (2026). https://doi.org/10.1038/s41598-026-38393-y

Jian Chen, Yukun Fan, Wanglu Jia, Haizu Zhang, Jie Xu, Ning Chen, Tao Mo, Xiaolin Hou, Yunpeng Wang & Ping'an Peng

Water geochemistry in the Bozhi-Dabei area, Tarim Basin and its implications for natural gas accumulation in deep basin

Jian Chen[1,2*], Yukun Fan[3], Wanglu Jia[1,2], Haizu Zhang[4], Jie Xu[1,2,5], Ning Chen[3], Tao Mo[4], Xiaolin Hou[3], Yunpeng Wang[1,2,5], Ping'an Peng[1,2,5]

[1] State Key Laboratory of Deep Earth Processes and Resources, Guangzhou Institute of Geochemistry, Chinese Academy of Sciences, Guangzhou 510640, China

[2] CAS Center for Excellence in Deep Earth Science, Guangzhou 510640, China

[3] Xi'an AMS Center, State Key Laboratory of Loess Science, Shaanxi Key Laboratory of Accelerator Mass Spectrometry Technology and Application, Institute of Earth Environment, Chinese Academy of Sciences, Xi'an 710061, China

[4] Research Institute of Petroleum Exploration and Development, PetroChina Tarim Oilfield Company, Korla 841000, China

[5] University of Chinese Academy of Sciences, Beijing 100049, China

* Corresponding author chenjian@gig.ac.cn

Abstract

Recently, numerous gas fields have been discovered in deep basins worldwide. However, the geochemistry of the produced water has been poorly studied. Here, we present the chemical and isotopic compositions of water produced from the deep (4–7 km) Bozhi–Dabei (BD) gas field, Tarim Basin, China. The data indicate that the produced water is a mixture of formation water and water condensed from gas. The latter of which has contents of lower total dissolved solids (TDS), different ionic compositions and more negative δD and δ^{18}O values than that of formation water. The formation water in the Lower Cretaceous sandstone reservoirs consists mainly of meteoric water that was strongly affected by the dissolution of Paleogene halite, forming a regional seal. Meteoric water infiltrated the Kumugeliemu halite during the Kangcun–Kuqa stage (16.3–1.64 Ma, Middle Miocene–Late Pliocene interval). A smaller portion of the formation water consists of iodine-rich evaporated seawater that migrated together with gas from transgression-influenced layers in Triassic–Jurassic source rocks. Using the ^{129}I dating model, different episodes of this migration in the Dabei (DB) East District were recognized, although the dating results were not precise. This study enhances our understanding of the migration and accumulation processes of formation water and natural gas in deep basins and suggests that the chemical and isotopic composition of formation water can be used together with that of gas to constrain the sources and accumulation processes of deeply buried gas.

Keywords: gasfield water; iodine-129; oil-water relationship; Tarim Basin; gas accumulation

In the field of petroleum geology, one of the most important research objectives is to correlate the sources of hydrocarbon accumulations with potential petroleum sources and elucidate the migration and accumulation processes of the accumulated hydrocarbons. However, previous studies have focused on the hydrocarbons themselves[1-3], and little attention has been given to water, which is also a major geological fluid in petroleum-generating basins. With the continued development of the petroleum industry, interest in the water produced during petroleum recovery has increased[4-6]. Numerous components in produced water provide insight into the sources, migration, and accumulation processes of hydrocarbons[7-9]; notably, water is involved in many hydrocarbon-related geological events, such as the maturation of source rocks, expulsion and migration of hydrocarbons, and hydrocarbon alteration in reservoirs[10-12]. During these processes, some hydrocarbon-related components with specific geochemical characteristics (e.g., iodine, organic acid, and lithium-6) are likely to be distributed in the water as a result of hydrocarbon–water–rock interactions[7,13,14]. Among them, iodine (I) is unique. As a biophilic species, it serves as a proxy for hydrocarbon migration, and iodine-129 (^{129}I), the only long-lived radioisotope of I, can be used to constrain hydrocarbon accumulation times[15,16]. The ^{129}I dating approach can provide precise accumulation times for hydrocarbons, times that cannot be obtained through conventional organic geochemical analyses. Although the ^{29}I dating technique has been adopted in numerous case studies, these studies focused on shallow reservoirs (e.g., gas hydrate occurrences and oil accumulations[17-19]) rather than on deep basins where gas accumulations are more likely to be found.

With petroleum exploration involving deeper strata, many gas reservoirs have been discovered worldwide[20,21]. However, only a few studies involving the geochemistry of the water produced in gas fields have been conducted[22-24]. In these studies, investigators sought to distinguish formation water from condensed water, explain the origins and evolution of formation water, and estimate reservoir temperatures using chemical geothermometers. However, the relationships between gas and water have not been explored. Both fluids can migrate together under certain geological conditions. For example, if fault systems link the source rocks and reservoirs and begin opening when petroleum expulsion begins, both the hydrocarbons and pore water in the source rocks may migrate into reservoirs along the fault system. Therefore, the formation water in gas field reservoirs may contain specific hydrocarbon-related information. Detailed geochemical research on the water produced from gas fields would provide additional information on the origin and migration of natural gas.

In this study, a series of water samples were collected from gas-producing wells in the Lower Cretaceous sandstone reservoirs of the Bozhi–Dabei (BD) gas field in the Tarim Basin, northwestern China. The chemical components and several isotopes (e.g., δD, $\delta^{18}O$, and $^{129}I/I$) were systematically analyzed. First, formation water was distinguished from condensed water in terms of its chemical and isotopic compositions with the aid of production data. The sources, migration, and evolution processes of the formation water were then revealed. Finally, a dating model based on the geochemical behavior of ^{129}I was constructed to reveal the different migration episodes of both natural gas and related water in a specific district. This research

could enhance our understanding of the migration and accumulation processes of formation water and natural gas in deep basins.

Geological setting

The Kuqa Depression, which is located in the northern part of the Tarim Basin (Fig. 1a), consists of eight tectonic subunits called the “Five Belts and Three Sags”: the Northern Monoclinal Belt, Kelasu Fold Belt, Yiqikelike Fold Belt, Qiulitage Fold Belt, Southern Gentle Monoclinal Belt, Baicheng Sag, Wushi Sag, and Yangxia Sag (Fig. 1b). This depression is filled mainly with Mesozoic and Cenozoic clastic sediments. Salt sequences are present in the Paleogene Kumugeliemu Formation in the western and middle parts of the Kuqa Depression and in the Neogene Jidike Formation in the eastern part of the depression[25,26]. Thus, the Mesozoic and Cenozoic strata are typically divided into three sequences (e.g., suprasalt, intrasalt, and subsalt[27,28]; Fig. 1d, Fig. 2). The Paleozoic and Precambrian strata are deeply buried and, thus, are poorly understood.

The Kuqa Depression is a superimposed Mesozoic and Cenozoic foreland basin that developed along a passive Paleozoic continental margin[29]. The evolution of the foreland basin can be divided into three stages: a back-arc foreland basin stage (Triassic), a fault depression–depression basin stage (from the Jurassic to the Paleogene), and a combined rejuvenated foreland basin stage (Neogene to Quaternary)[30,31]. The structures in the Kuqa Depression are characterized by a series of thrust belts and fault-related folds. They formed as a result of strong compression and thrusting that were driven by the intracontinental subduction of the Tianshan

Orogenic Belt since the Miocene[31,32]. These thrust faults act as major pathways for hydrocarbon migration, and fault-related folds are favorable zones for oil and gas accumulation.

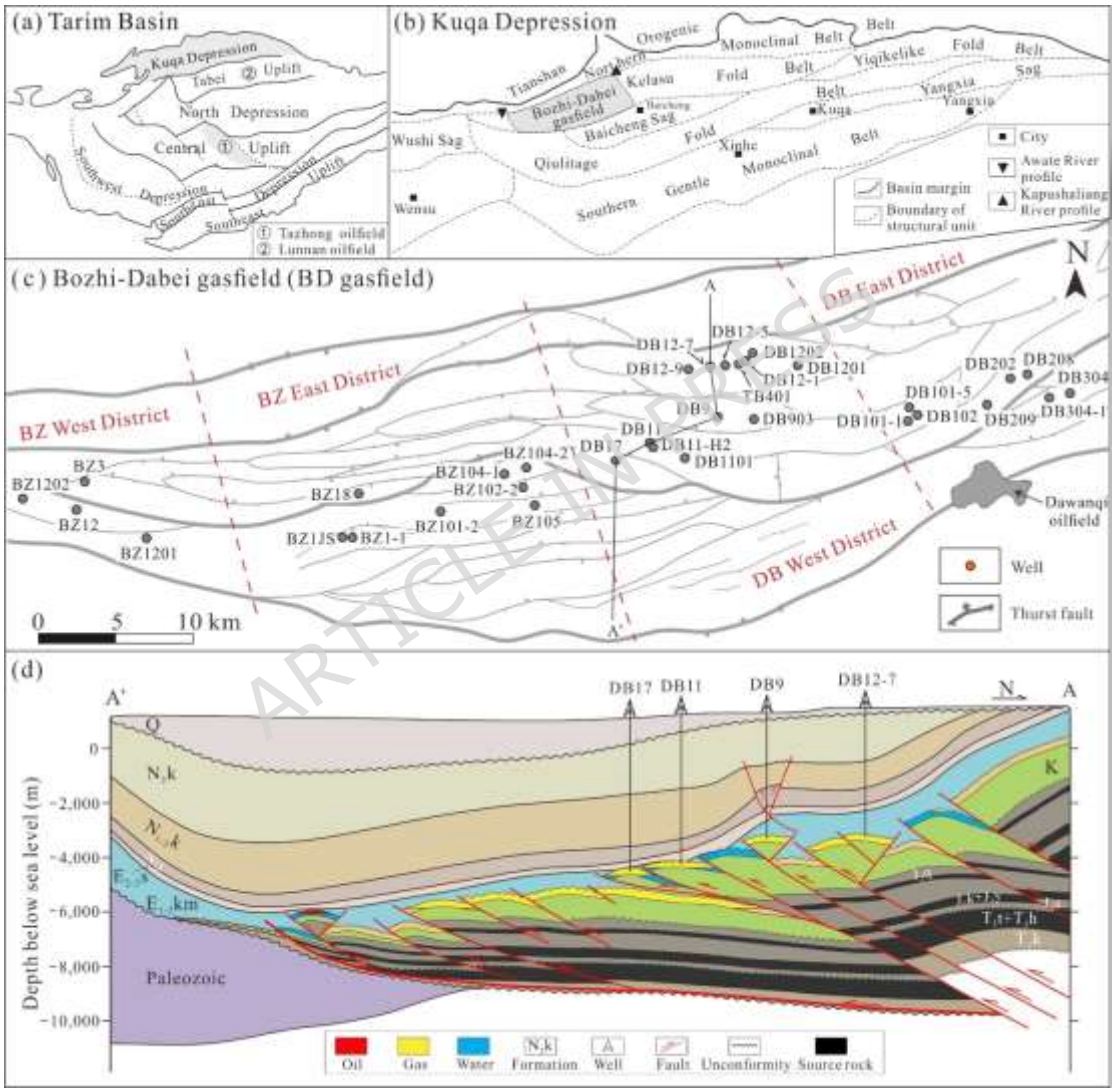

Figure 1. Structural map of the Tarim Basin (**a**), Kuqa Depression (**b**) and Bozhi–Dabei (BD) gas field (**c**) and cross-section along line A–A' (**d**, modified from Mo et al.[33]).

Note: The locations of the Tazhong oilfield and Lunnan oilfield in the platform region

of the Paleozoic craton are shown in Panel a. For the purpose of analysis and discussion, the study area was divided into four districts (BZ West District, BZ East District, DB West District and DB East District, Panel **c**).

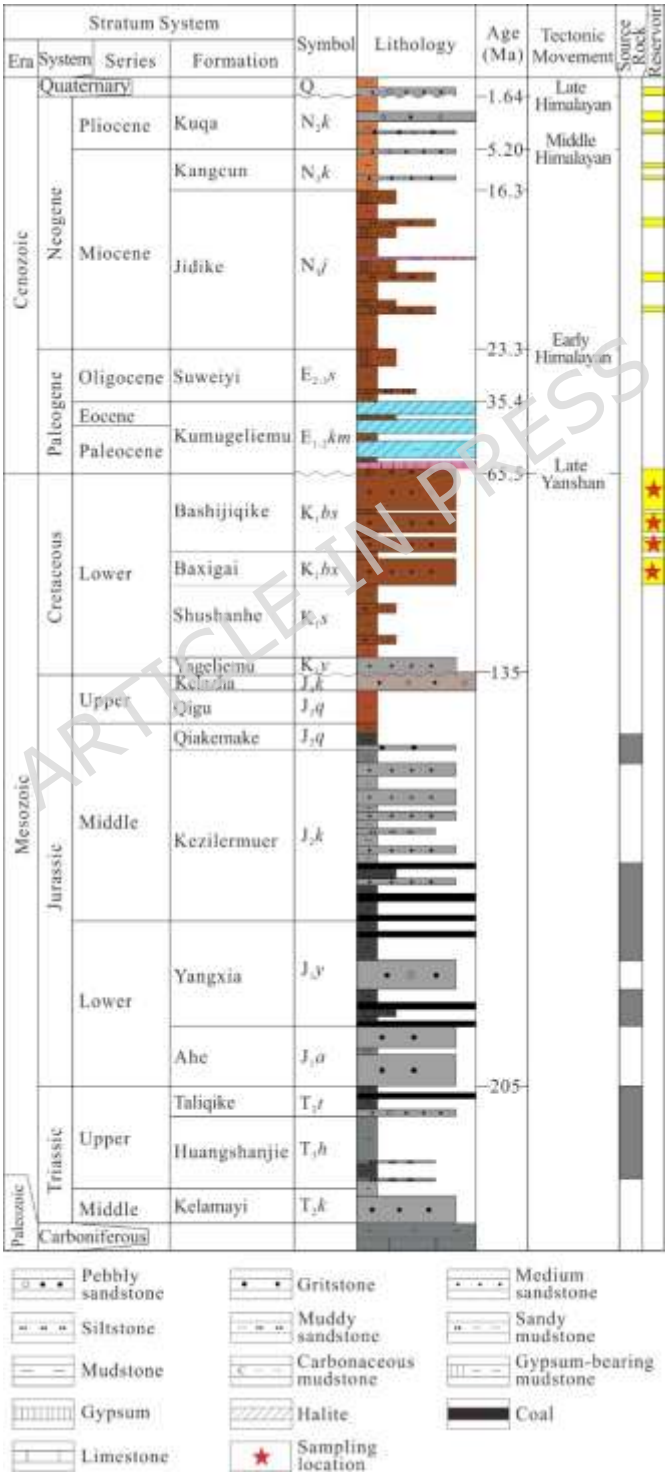

Figure 2. Simplified stratigraphic column of strata in the BD gas field, Kuqa Depression.

The coal and lacustrine mudstones in the Triassic and Jurassic sediments represent two series of major source rocks. The mudstones are composed of type II–III kerogens, whereas the organic matter in the coal consists mainly of type III kerogen[34]. The Triassic source rocks reached an oil-generating peak at the end of the Paleogene, whereas the Jurassic source rocks began to generate oil during the Miocene[34,35]. With rapid burial after the deposition of the Kuqa Formation (< 5.20 Ma), both source rocks entered gas generation stages[34,36]. At present, the source rocks in the depositional centers have reached a high and overmature stage (Ro>2.2%)[36,37]. The Lower Cretaceous sandstones, including the Bashijiqike (K_1bs) and Baxigai (K_1bx) Formations, are the major gas reservoirs and are dominated by fine- to medium-grained lithic arokoses and feldspathic litharenite, which were deposited in a fan-braided deltaic progradational setting[38-40]. The Kumugeliemu salt sequences formed excellent regional seals in the western and middle regions of the Kuqa Depression. They formed in saline lacustrine environments[36] but were possibly influenced by sea invasion from the Neo-Tethys Ocean[41,42].

The BD gas field is located to the west of the Kelasu Fold Belt, Kuqa Depression. Gas is the major type of hydrocarbon produced; however, various forms of oil are also found. Most Dabei wells are in the dry gas stage, whereas the wells in the Bozi Block are characterized by wet gas and condensate pools (Table S1). Studies of hydrocarbon-bearing inclusions have shown that the K_1 reservoirs of the east region

of the BD gas field contain one form of single-phase CH_4-rich inclusion and two types of oil inclusions with blue–white and yellow–white fluorescence, respectively[43,44]. By combining the results of burial and thermal history modeling with homogenization temperature data (Th) of the aqueous inclusions, an oil charging episode was estimated to have occurred at 5–4 Ma, and a gas charging episode was likely to have occurred at 3–2 Ma. Another oil charging episode was not identified because of the inability to obtain Th data for the coeval aqueous inclusions. The yellow–white fluorescence of these oil inclusions, however, indicated that the oil was at a relatively low maturity stage, and this oil charging episode should have taken place at an earlier time (>5 Ma)[43,44]. Most oils remigrated after oil accumulation. Some of these oils were lost, while others accumulated again in Neogene–Quaternary reservoirs to form the Dawanqi oilfield (Fig. 1c)[45].

Samples and methods

All water samples were collected from Lower Cretaceous sandstone reservoirs (K_1bs and K_1bx) at depths of 4,802–7,317 m below sea level (Fig. 1c). Only water samples from gas wells that had been in active production for at least six months were collected; thus, any contamination from drilling additives was avoided. At the sampling site, the collected water samples were filtered through 0.45-μm Millipore filters and collected in clean plastic bottles.

Total dissolved solids (TDS) were measured using the gravimetric method described by Clescerl et al.[46]. The chloride (Cl), bromide (Br) and sulfate (SO_4)

concentrations were measured by ion chromatography following appropriate dilution with a Dionex AQUION RFIC instrument, an AS19 ion exchange column and 10 mM KOH eluent. The relative analytical uncertainty was greater than 3.0%. The quantity of iodine (I) was measured using an 8800 inductively coupled plasma–mass spectrometer (ICP–MS; Agilent Corporation, USA). Replicate analyses yielded a precision > 4%. The sodium (Na), potassium (K), calcium (Ca), and magnesium (Mg) concentrations were measured by ion chromatography following appropriate dilution with a Dionex ICS 900 instrument employing a CS12 ion exchange column and 9 mM methanesulfonic acid eluent. The relative analytical uncertainty was greater than 5.0%. Trace elements, including barium (Ba), strontium (Sr), and lithium (Li), were analyzed in diluted solutions using a Varian Vista-Pro ICP optical emission spectrometer (ICP–OES) with an analytical uncertainty greater than 5%.

The δD and δ^{18}O isotopic compositions were analyzed using a Picarro L2130-I isotopic water analyzer, and the isotopolog concentrations were determined using cavity ringdown spectroscopy. The δD and δ^{18}O values were recorded relative to those of Vienna standard mean ocean water (V-SMOW). Replicate analyses yielded precisions of ±0.4‰ and ±0.1‰ for δD and δ^{18}O, respectively. Iodine was separated from water as AgI using an improved solvent extraction procedure[47-49]. The ^{129}I/I ratios in the AgI precipitates were measured via accelerator mass spectrometry (AMS) using a 3-MV tandem AMS system. The measured ^{129}I/^{127}I values of the blank samples were approximately 2×10^{-13} and were subtracted from those of the actual samples, which were at least three times greater than those of the blanks.

Results

The range of TDS concentrations was 5.59 to 264.10 g/L (Table S1). On the basis of the definition of water salinity[5,50], the water samples were classified as brine (>35 g/L; 16 samples), saltwater (10–35 g/L; 12 samples), or brackish water (1–10 g/L; 5 samples). The water obtained from the DB East District was generally more saline than the water from the other districts were. In most water samples, Cl and Na were the predominant anion and cation, respectively. However, SO_4 was the predominant anion in three water samples (BZ12, BZ1201, and BZ1202), with concentrations ranging from 3,637.80 to 8,183.00 mg/L. The chemical compositions of these water samples were broadly consistent with previously published data for oilfield water[4-6].

As shown in the Piper diagram (Fig. 3a), most water samples were grouped in the Cl and Na+K corners and were classified as Na–Cl-type water. The exceptions were BZ12 and BZ1201 (Na-SO_4 type). Consistent with the Piper diagram, most water samples were dominated by Cl and Na in the Schoeller diagram, with BZ12 and BZ1201 as exceptions (Fig. 3b). Interestingly, most of the water samples (in either the Piper or Schoeller plots) were characterized as close to seawater; that is, some were similar to the brine in the deep reservoirs of the platform region of the Paleozoic craton, Tarim Basin[51,52], although they were collected from deltaic sandstone reservoirs. In addition, the evident disparity between water samples obtained from local surface water[53,54] indicated that these produced water samples were not contaminated by drilling additives, which are commonly mixed with local surface water during drilling operations.

The δD values varied between -94.82‰ and -53.76‰, and the $\delta^{18}O$ values were mostly positive, ranging from -5.83‰ to 2.98‰. Both values are very different from those of seawater (0‰ and 0‰) or local surface water (-82% to -70% and -12.2% to -10%)[53,54], which suggests a mixed origin for the water and possibly strong water–rock interactions. The $^{129}I/I$ ratios in all the water samples varied between 296 and 4,870 $\times 10^{-15}$. These ratios are significantly lower than those in the surface environment after the nuclear era (typically > 10,000 × 10^{-15})[7], thus suggesting that anthropogenic ^{129}I inputs in these water samples are negligible and that contamination during the sampling protocols was prevented.

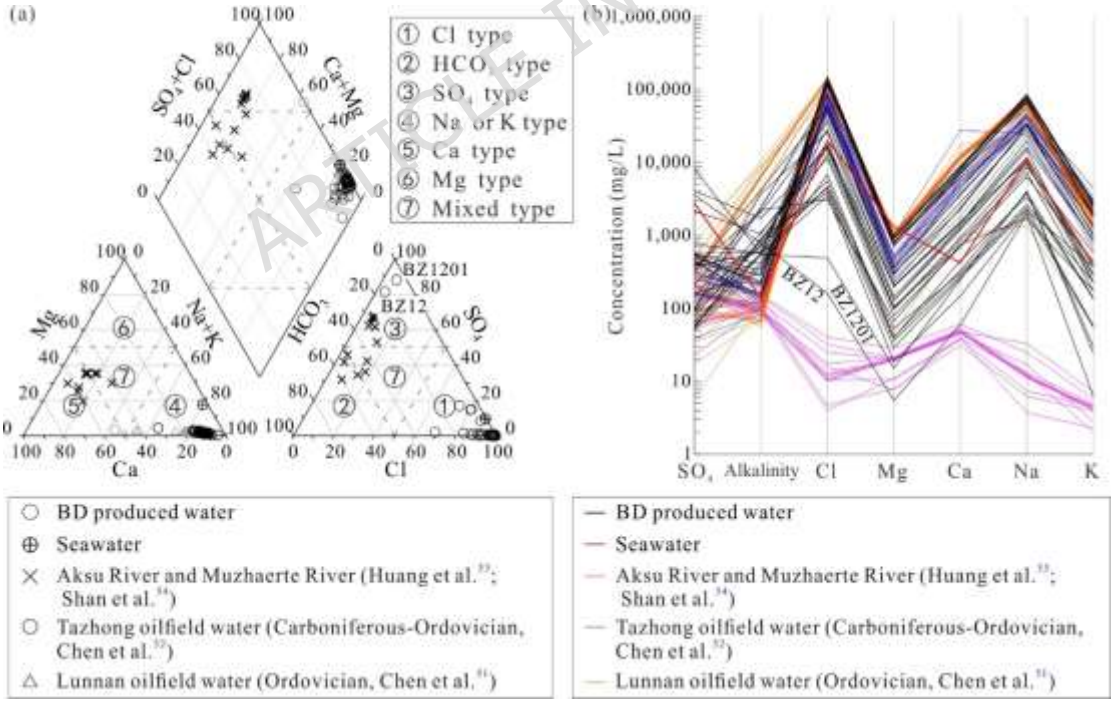

Figure 3. Piper (**a**) and Schoeller (**b**) diagrams of the produced water in the BD gas field.

Discussion

Influence of condensed water

Condensed water accounts for a certain proportion of the produced water in gas reservoirs—especially in reservoirs with high gas–water ratios (GWRs)—and is thus an important factor in determining the origin of formation water, which is in the liquid phase in reservoirs[22,24,55]. Accordingly, we sought to estimate the influence of condensed water on the produced water that was obtained from the study wells. The TDS contents of the produced water were negatively correlated with the GWRs (Fig. 4a). The produced water samples that were associated with high gas yields had low TDS values. Lico et al.[56] suggested that water produced at gas wells with GWRs <30,000 m^3/m^3 is not diluted by condensed water. On the basis of these criteria, only six water samples in the DB East District (DB101-1, DB101-5, DB102, DB208, DB209, and DB304) were classified as formation water; the other water samples were diluted by condensed water to varying degrees. As evidenced by the well production logs (Fig. 4b), the TDS levels in the produced water in the early stage of gas well production were relatively low but increased with continued gas production. These findings are consistent with the results of previous studies, which suggest that the invasion of formation water with increasing gas production could decrease the GWR and thus reduce the proportion of condensed water in the produced water[22,24].

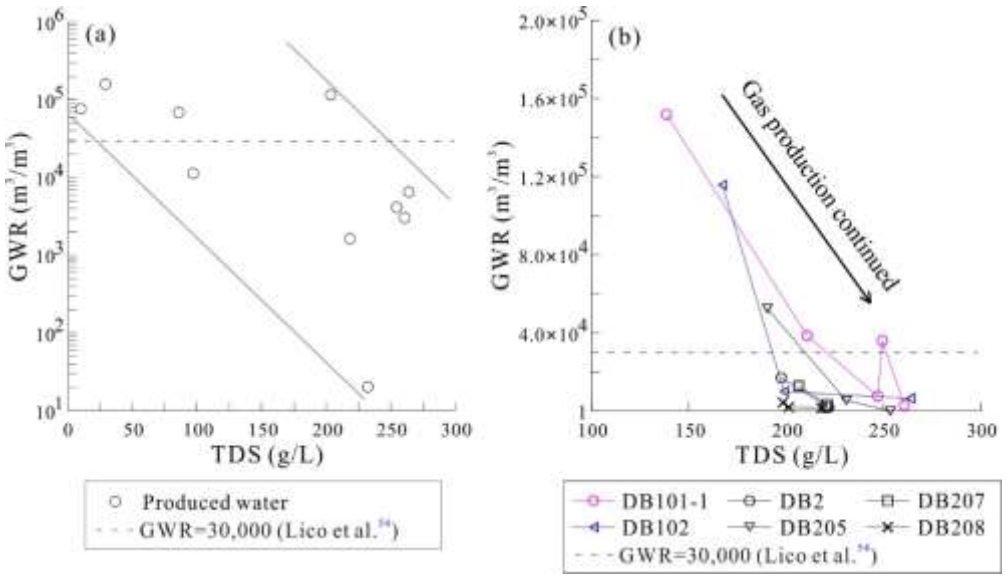

Figure 4. Relationships between the gas-to-water ratio (GWR, m^3/m^3) and total dissolved solids (TDS, g/L) in the sampling wells in this study (**a**) and from well production logs (**b**) from the BD gas field.

Condensed water is considered to have low salinities and relatively low isotopic compositions[22,57]. In the BD gas field, five samples of brackish water (DB1202, DB11, DB17, BZ1JS, and BZ12) had significantly lower TDS (5.59 to 9.72 g/L) and negative δD (-75.08 to -65.22‰) and δ^{18}O (-4.06 to -1.62‰) values than the other samples did (96.94 to 264.10 g/L of TDS, -59.82 to -53.76‰ of δD, 0.64 to -2.98‰ of δ^{18}O). The isotopic compositions of condensed water were controlled mainly by temperature-dependent equilibration fractionation. According to the equilibration fractionation equation of Horita & Wesolowski[58], the condensed water that equilibrated with the formation water in reservoirs had theoretical δD and δ^{18}O values (-78.11‰ to -72.00‰ and -2.81‰ to -1.13‰, respectively), similar to the measured values for one of the brackish water

samples (BZ12, which had the lowest δD value of all the brackish water samples). As such, the five brackish water samples from the BD gas field can be considered condensed water. In terms of ionic compositions, these condensed water samples were relatively enriched in HCO_3 and SO_4 and depleted in Cl, and the ranges of K, Na, Ca, and Mg were more variable than those in the formation water samples were (Fig. 5a and 5c). The reason for this ionic composition was not clear. The ionic compositions of condensed water are controlled by numerous geological and gas-production-related processes (e.g., ion partitioning between vapor and liquid water, dissolution from adjacent minerals, and contact behavior among water, hydrocarbons, and rocks)[55]. However, low salinity has always been considered a typical characteristic of condensed water.

The ionic compositions of the formation water and condensed water differed from those of the local surface water (Fig. 5a and 5c); the formation water was very similar to the brine present in the deep reservoirs of the platform region of the Paleozoic craton, Tarim Basin, except for the low content of Ca in the formation water (Fig. 5a). Furthermore, other water samples exhibited mixed compositional characteristics, such as combined formation water and condensed water, and thus were considered mixed water (Fig. 5b).

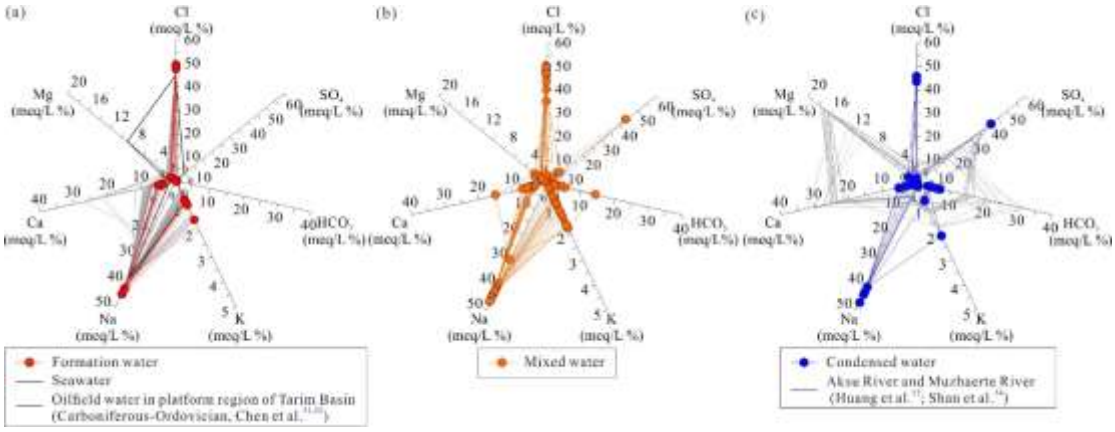

Figure 5. Major ionic compositions of the formation water (**a**), mixed water (**b**) and condensed water (**c**) in the BD gas field.

Two endmembers of formation water

The water samples from the BD gas field are distributed on the right side of the global meteoric water line (GMWL) and far below the seawater and seawater evaporation trajectory (SET; Fig. 6). The formation water plotted in the same region as the water from the platform regions in the same basin, implying that they shared a similar origin. The water in the platform regions formed via the mixing of meteoric water and evaporated seawater, followed by a positive $\delta^{18}O$ shift during long-term water–rock interactions[51,52]. As such, the mixture of evaporated seawater and meteoric water could be a source of the formation water in the basin. The mixed water plotted in a region located between those where the formation water and local surface water (also local meteoric water) plotted. The condensed water plotted in the middle of the data cluster, and compared with the condensed water, some of the mixed water had lower δD and $\delta^{18}O$ values. It appears that another recent

meteoric water influx likely occurred in the mixed water reservoir. If this was the case, recent meteoric water would have dissolved the E_{1-2}km halite as the water infiltrated downward and thus resulted in high salinity. However, the low TDS values of the mixed water contradict this explanation. Furthermore, the δD and δ^{18}O values of condensed water under geological conditions could be lower than the values that were calculated from the equilibration fractionation equation by Horita & Wesolowski[58] because the isotopic fractionation process is controlled not only by temperature but also by other factors (e.g., salinity, pressure, and isotopic exchange with other oxygen-containing and hydrogen-containing compounds). Therefore, the lower levels of δD and δ^{18}O isotopes in mixed water can be attributed to mixing with condensed water rather than a recent invasion of meteoric water.

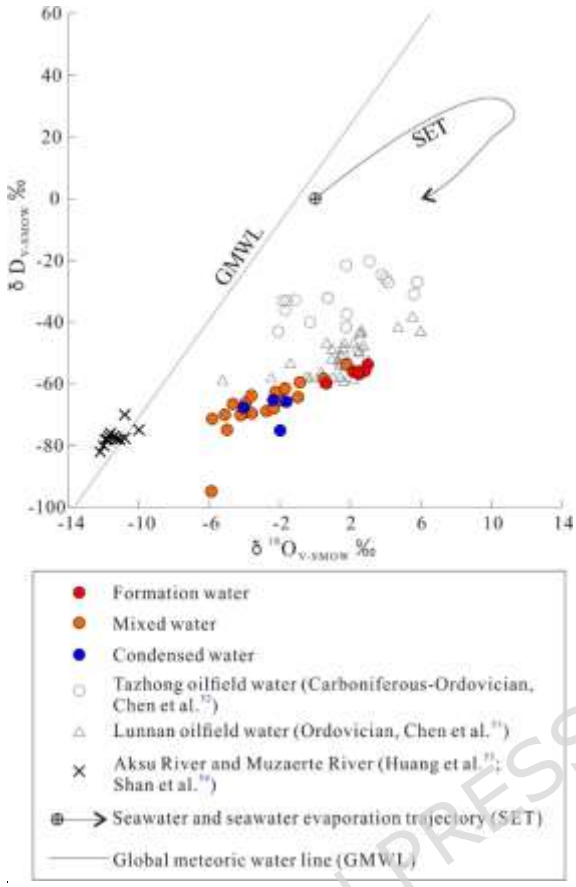

Figure 6. Plot of δD vs. $\delta^{18}O$ values of the produced water of the BD gas field.

Compared with seawater, the produced water had lower Br contents (1.00–42.31 mg/L) and higher Cl/Br mass ratios (1,719–16,320), as shown to the left of the SET in Fig. 7a. Among all the different types of water, formation water with high Cl and Br contents plotted in a region with halite-dissolution water. These findings indicate that the Cl and Br in the formation water were derived mainly from halite dissolution. Halite that is deposited in sedimentary basins typically has low Br concentrations (50–200 ppm) because of the low partitioning coefficient of Br into mineral lattices during halite precipitation[6,59]. Consequently, the dissolution of halite yields water with high Cl/Br ratios. However, halite-dissolution water is characterized

by variable Br contents (3.5–97 ppm) and high Cl/Br ratios (1,246–43,311 ppm)[60-62] because halogen partitioning behavior during halite precipitation and dissolution is controlled by many geological factors (e.g., source of solutes, stage of halite precipitation, and water–rock ratio when dissolution occurs)[6]. In the BD gas field, the endmember of evaporated seawater is characterized on the basis of the δD–$\delta^{18}O$ relationship. Therefore, the formation water is mixed with a high proportion of halite-dissolution meteoric water and a low proportion of evaporated seawater. Furthermore, the TDS values (96.94–264.10 g/L), which were lower than the solubility of sodium chloride in water (360 g/L at 25 °C), demonstrated that the formation water was not saturated with halite and that another type of water (evaporated seawater) contributed.

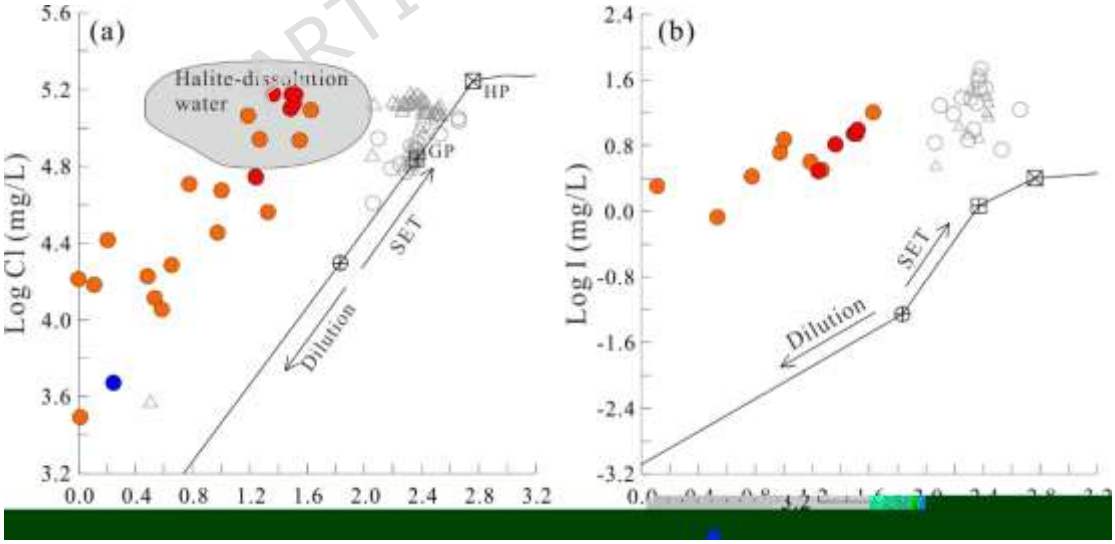

Figure 7. Plots of Cl vs. Br (**a**) and I vs. Br (**b**) for the produced water from the BD gas field. The seawater evaporation trajectory (SET) in both figures was generated using

data from Fontes and Matray[63] and Zherebtsova and Volkova[64]. “Dilution” indicates the dilution of seawater by freshwater. “GP” and “HP” indicate the stages in which gypsum and halite start to precipitate, respectively. Halite-dissolution water data were obtained from Kloppman et al.[60], Pinti et al.[61] and Worden et al.[62]. Other symbols are defined in Fig. 5.

The approximate proportions of halite-dissolution meteoric water and evaporated seawater were also calculated. If the δD values of local meteoric water (-80‰) and seawater (0‰) were selected as the endmembers, the contributions of meteoric water to formation water were between 67.2% and 74.7%. If the lowest content of Br in halite-dissolution water (4 mg/L[61]) and the Br content in evaporated seawater at the stage where gypsum began to precipitate (234 mg/L[63]) were selected as the endmembers, the ionic contribution of halite dissolution in the formation water ranged between 87.4% and 95.1%. Therefore, the major contribution of halite-dissolution meteoric water to the formation water was confirmed.

Origin of formation water

The iodine contents of the water samples (0.77–16.12 mg/L) were higher than those of the seawater and the SET (0.06 mg/L[64]); accordingly, the samples are plotted in the upper left zone of the SET in Fig. 7b. In sedimentary basins, the enrichment of I in water is not due to any kind of water–rock interaction because

the large ionic radius of I makes it difficult to incorporate into mineral lattices and instead is solely attributed to the degradation of organic material during source rock maturation because of the biophilic nature of I[6,65]. Therefore, such high amounts of iodine were not sourced from halite-dissolution meteoric water. However, it is unclear when I was released into the pore water in the source rock. Since the generated oils are universally depleted in I (0–23.1 mg/g oil[66-68]) in comparison to those from organic matter-rich (OM-rich) shales (195–6150 mg/g rock[69]), it is highly likely that the pore water from the source rock that was obtained after the oil window could already be rich in I. Thus, the seawater evaporated from the deep strata could be expelled from the mature source rocks or pass through the mature source rocks and thus participate in I uptake.

Although the Triassic–Jurassic source rocks were deposited in swamp and lacustrine settings, many OM-rich layers, including Qiakemake (J_2q), the upper layer of Yangxia (J_1y), and Huangshanjie (T_3h), have been demonstrated to have experienced Tethys Ocean invasion, and the quality of organic matter greatly increased in those instances[70,71]. Furthermore, both the oil–source correlation and the gas–source correlation in previous studies indicate that both hydrocarbon types in the BD gas field are humic organic matter and thus are confidently derived from Triassic–Jurassic source rocks[72-74]. As such, the evaporated seawater can be derived from OM-rich Triassic–Jurassic strata, which were influenced by seawater invasion. Paleozoic marine strata are another possible source of evaporated seawater. However, related geological information is generally limited because these strata are deeply buried at depths > 8,000 m,

and no drilling operations in the study area report the occurrence of Paleozoic marine strata. Although some Carboniferous sediments have been discovered in outcrops near the Tianshan Orogenic Belt, all are organic-lean rocks[25]. Furthermore, the inclusion analysis of the K_1 sandstone reservoirs indicates that the homogenization temperature of aqueous inclusions was never higher than 150 °C, which further indicates that hot fluids from Paleozoic marine strata did not occur[43,45]. In addition, the previous oil/gas correlation also excludes any fluid migration from Paleozoic marine source rocks, which should take plankton and bacteria as major biological inputs[72-74]. Therefore, on the basis of the present geological information, any fluid migration from Paleozoic strata is difficult to verify. Overall, the OM-rich layers that were influenced by seawater invasion in the Triassic–Jurassic strata were the most likely sources of I-rich evaporated seawater.

The evaporated seawater occupying the pores of OM-rich layers could take I up from kerogen and then migrate upward with natural gases during the maturation of source rocks. Previous studies have demonstrated that OM-rich shale can contain a certain amount of connate water (water saturation > 10%) after compaction during the diagenetic stage[75-76]. These water molecules are stored in organic and inorganic pores with diverse pore widths, mainly through monolayer adsorption[77]. However, the water content evolves with both hydrocarbon maturation and mineral transformation. Thermal simulation of a selected shale core sample revealed that the water content in this OM-rich shale varied greatly (9.77–32.20 mg/g rock)[78]. The increase in water content during the

thermal simulation was attributed to the release of water from clay transformation, including the illitization of smectite and degradation of kaolinite, whereas two reductions in water content during the maturation process indicated two coexpulsion events for both pore water and hydrocarbons (pore water plus oil and pore water plus natural gas, respectively). The displacement of liquid and gaseous hydrocarbons is the major driving force for water expulsion. In terms of the BD gas field, a certain amount of evaporated water as connate water could be retained in the pores of OM-rich layers that were influenced by seawater invasion and then take I up from kerogen during the maturation process. Afterward, with the further maturation process, some of the I-rich evaporated water was expelled with generated crude oils, whereas the others migrated outside the source rock with natural gases during the late period. The water released from clay transformation was suggested to be fresh[79-80], but its ionic composition was not clear. The high TDS content of the formation water of the BD gas field suggested that the contribution of water released from clay transformation might be very limited.

In the BD gas field, the Kumugeliemu salt sequence (E_{1-2}km) contains several layers of gypsum-bearing mudstone, gypsum, and halite, with a total salt thickness of 100–3,000 m. This sequence was deposited in a lagoon environment but was influenced by invasion from the Neo-Tethys Ocean, which flooded the Tarim Basin via the Awati Strait to the west[41,42]. The meteoric water would have infiltrated downward—dissolving halite after the E_{1-2}km salt sequences were deposited. However, the evaporated seawater, as another endmember of the

formation water, could not be derived from the residual seawater if it was trapped in the E_{1-2}km halite. Such a mixture of residual seawater and halite-dissolution meteoric water could not explain the enrichment of I in the formation water. As such, the residual seawater in E_{1-2}km could be displaced after halite precipitation and thus did not contribute to the formation of water. The deep source of the evaporated seawater is again confirmed. The connate water in the reservoirs was of meteoric origin, as evidenced by the fact that the Lower Cretaceous sandstone was deposited in a fan-braided deltaic progradational setting, but the water in this environment might have been saline or brackish because of evaporation in a tropical and arid paleoclimate[38,40]. However, the connate water should have been displaced by meteoric water during the denudation period in the Late Cretaceous. Here, the high TDS content of formation water indicated that both connate water and meteoric water with fresh characteristics were highly likely to be displaced by later geological fluids and thus did not remain. Therefore, the formation water was likely mixed with large proportions of meteoric water that infiltrated the E_{1-2}km halite, and a small proportion of I-rich evaporated seawater migrated upward from OM-rich Triassic–Jurassic source rocks. During gas production, formation water was mixed with condensed water in most wells—to varying degrees—to form mixed-source water.

Evolution process of formation water

The evolution process of the formation water was strongly related to the maturation history of the Triassic–Jurassic source rocks and local tectonic events. Six source layers in the extensive Triassic and Jurassic strata were demonstrated to sequentially generate oil from the end of the Paleogene to the end of the Miocene (65.5–5.20 Ma)[34,35]. At nearly the same time, with compression by the Tianshan Orogenic Belt, large-scale thrust faults began to develop from north to south in the Kuqa Depression, and some low-amplitude anticlines developed on the tops of the thrusts[73]. The thrust faults linked these source layers to traps and thus provided effective migration pathways for the expelled oil. Consequently, oil accumulated in the K_1 sandstone reservoirs, with the $E_{1\text{-}2}$km salt as the seal. During the Middle Miocene to the Pliocene (Kangcun–Kuqa stage, 16.3–1.64 Ma), thrust fault systems developed further, and the $E_{1\text{-}2}$km salt began to experience plastic flow. Some thrust faults penetrate thin sections of the $E_{1\text{-}2}$km salt layer. At this time, oil charging continued, but most of the accumulated oil migrated upward through the $E_{1\text{-}2}$km salt. From the Pliocene to the present (< 5.20 Ma), with the strengthening of thrust faults, a series of imbricated fault-block traps developed. The source rocks rapidly generated natural gas under the massive deposition of Kuqa and Quaternary strata (Pliocene to present, < 5.20 Ma). These gases migrated upward and accumulated in subsalt sandstone reservoirs to form the present DB gas field[45,73].

An endmember of formation water, namely, halite-dissolution meteoric water, likely intruded into reservoirs during the Middle Miocene to the Pliocene (Kangcun–Kuqa stage, 16.3–1.64 Ma) when the accumulated oil in the K_1 sandstone

reservoirs was altered. The thrust faults penetrating the E_{1-2}km salt layer provided the opportunity for the halite-dissolution meteoric water to move downward, a mechanism similar to that of the upward-migrating crude oils. Another endmember, namely, evaporated seawater, may have migrated together with natural gas from the source rocks rather than with crude oil. As mentioned above, the early-charged oils in the K_1 reservoirs were altered from the Middle Miocene to the Pliocene (Kangcun–Kuqa stage, 16.3–1.64 Ma), after which the reservoirs were filled with natural gas from the Pliocene to the present (< 5.20 Ma). Under these conditions, brine that migrated with crude oil could be largely displaced by late-charging fluids (e.g., halite-dissolution meteoric water migrating downward and water migrating upward with natural gas). Research on fluid inclusions has demonstrated that aqueous inclusions associated with late-charging gas (TDS; 150–250 g/L) are more saline than aqueous inclusions associated with early-charged oils (TDS<127 g/L)[43,44]. The former values are highly consistent with the measured salinity of the formation water in this study (TDS; 218.31–264.10 g/L, with the exception of 96.94 g/L). Therefore, the comigration of evaporated seawater and natural gas was confirmed.

The chemical composition of the formation water was diagenetically altered to a large degree. In addition to the halite dissolution mentioned above, the interactions were dominated by those with different kinds of clastic minerals; thus, the enrichment of Li and K and, partly, the enrichment of Ca in the formation water occurred (see Supplementary materials, Fig. S1). However, because the clastic sediments were distributed in all the Mesozoic–Cenozoic strata in the BD gas field, it is not clear in which strata these interactions occurred.

Dating model to constrain the migration times of evaporated water in the DB East District

Iodine-129 (^{129}I, $t_{1/2}$=15.7 Myr) is the only long-lived I radioisotope. Under natural conditions, ^{129}I can be generated by the spallation of Xe isotopes in the atmosphere (cosmogenic mode) and the spontaneous fission of ^{238}U in the crust (fissiogenic mode)[7]. Cosmogenic ^{129}I is homogeneous in all surface reservoirs, with an initial prenuclear equilibrium ^{129}I/I ratio of 1,500 × 10^{-15} [81]. When a fluid is isolated from the surface environment, ^{129}I decays as follows:

$$R = R_i e^{-\lambda_{129} t}$$

Equation (1)

where R is the ^{129}I/I ratio of the sample, R_i is the initial ^{129}I/I ratio (1500×10^{-15}), λ_{129} is the decay constant of ^{129}I (4.41×10^{-8} yr^{-1}), and t is the time elapsed since isolation.

During burial, the proportions of fissiogenic ^{129}I in the fluids increased. The abundance of fissiogenic ^{129}I was calculated using the following equation[82]:

$$N_{129} = N_{238}\boldsymbol{\lambda}_{238} Y_{129} \rho (E/P)\left(1 - e^{-\boldsymbol{\lambda}_{129} t}\right)/\boldsymbol{\lambda}_{129}$$

Equation (2)

where N_{129} is the number of ^{129}I atoms in a fluid sample, N_{238} is the number of ^{238}U atoms in a rock sample, λ_{238} is the decay constant for the spontaneous fission of ^{238}U (8.5×10^{-17} ·yr^{-1}), λ_{129} is the decay constant of ^{129}I (4.41×10^{-8} ·yr^{-1}), Y_{129} is the production rate for mass 129 (0.0003), ρ is the rock density, E is the proportion of

fissiogenic ^{129}I released from the rock, *P* is the effective porosity of the rock, and *t* is the time that the fluid has been in contact with the rock.

Because the dilution effects of condensed water in mixed water were not quantitatively evaluated, the assessment of ^{129}I data focused on the water samples in the DB East District, encompassing all the formation water samples and two other mixed water samples (DB304-1 and DB202). DB304-1 and DB202 might be influenced by dilution water to some degree because of their higher TDS contents and greater quantities of positive δD-$\delta^{18}O$ isotopes than those of other mixed water. The ^{129}I concentrations in the DB East District ranged between 12.42 and 42.90 atoms/μL and increased with a roughly west-to-east trend (Fig. 8). The ^{129}I concentrations were higher than those in prenuclear meteoric water (approximately 0.07 atom/μL[83]). This indicates another contribution from fissiogenic ^{129}I from rocks.

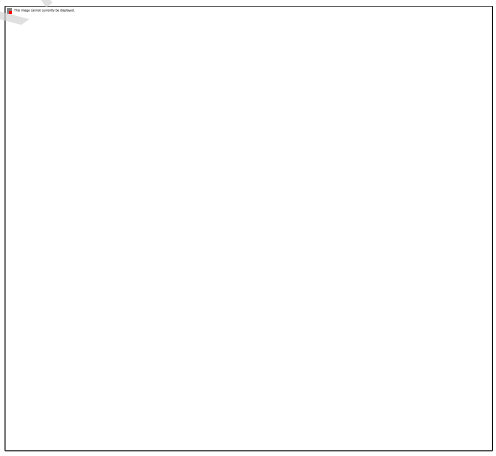

Figure 8. ^{129}I distributions in water samples from the BD East District. The sample symbols are defined in Fig. 5.

These water samples are mixed with deep evaporated seawater and halite-dissolution meteoric water. Halite-dissolution meteoric water received cosmogenic ^{129}I before moving downward. Evaporated seawater can obtain fissiogenic ^{129}I from U-enriched source rocks. ^{129}I from both meteoric water and evaporated seawater could have been delayed after both fluids entered the reservoirs. However, both meteoric water and evaporated seawater could obtain fissiogenic ^{129}I from the surrounding sandstone reservoirs. In conclusion, the ^{129}I concentrations in the water from the DB East District were composed of 1) cosmogenic ^{129}I in meteoric water, 2) fissiogenic ^{129}I from sandstone reservoirs in meteoric water, 3) fissiogenic ^{129}I from source rocks in evaporated seawater, and 4) fissiogenic ^{129}I from reservoirs in evaporated seawater. These relationships can be expressed using the following equation in four parts:

$$C_{129} =$$
$$(1-x)N_{MW129}e^{-\lambda_{129}t_{MW}} +$$
$$(1-x)N_{R238}\lambda_{238}Y_{129}\rho_R(E_R/P_R)(1-e^{-\lambda_{129}t_{MW}})/\lambda_{129} +$$
$$xN_{S238}\boldsymbol{\lambda}_{238}Y_{129}\rho_S(E_S/P_S)\left(1-e^{-\boldsymbol{\lambda}_{129}t_{eq}}\right)/\boldsymbol{\lambda}_{129}e^{-\lambda_{129}t_S} +$$
$$xN_{R238}\lambda_{238}Y_{129}\rho_R(E_R/P_R)(1-e^{-\lambda_{129}t_S})/\lambda_{129}$$

Equation (3)

where C_{129} is the measured ^{129}I concentration in water; x is the proportion of evaporated seawater; N_{MW129} is the number of ^{129}I atoms in prenuclear meteoric water in an equilibrium state; t_{MW} and t_S are the times the meteoric water and evaporated seawater entered the reservoir, respectively; N_{R238} and N_{S238} are the numbers of ^{238}U atoms in the reservoir and source rocks, respectively; ρ_R and ρ_S are

the densities of the reservoir and source rocks, respectively; E_R and E_S are the proportions of fissiogenic ^{129}I released from the reservoir and source rocks, respectively; P_R and P_S are the effective porosities of the reservoir and source rocks, respectively; and t_{eq} is the time the evaporated seawater contacted the source rocks before being expelled.

In Equation (3), t_S is an unresolved parameter. To calculate t_S, the following data were used: x was calculated using the δD value of the formation water, and -80‰ and 0‰ were assumed to be the endmembers of meteoric water and evaporated seawater, respectively. The calculated x values varied between 25.0% and 30.2% (Table S2). N_{MW129} was 0.074 atoms/μL, as obtained by multiplying the number of I atoms in meteoric water (4.95×10^{10} atoms/μL[84]) and R_i (1500×10^{-15} [74]). The t_{MW} values ranged between 16.3 and 1.64 Ma according to the above discussion. N_{R238} was 4.02×10^{18} atom/kg, which was calculated from the average U content in the K_1bs sandstone (1.59 mg/kg; n=9[85]). Because the shales and coals in the Triassic–Jurassic strata have been suggested to generate natural gas in the BD gas field[73,86], the average U content of both types of source rocks (4.37 mg/kg; n=35; measured in this study; Table S3) was used to calculate N_{S238} (1.11×10^{19} atom/kg). ρ_R is 2.60 g/cm^3 for sandstone[48]. The ρ_S values should vary between 1.50 and 2.60 g/cm^3, which are the average densities of anthracite (high-rank coal)[87] and black shale[15], respectively. The E/P ratio was used to indicate the escape probability of ^{129}I from the rock into fluids. This parameter cannot be obtained precisely but was commonly assumed to be in the range of 1–30 in previous studies[7]. It is believed that ^{129}I can escape from source rocks into pore water rather easily because compared with U in mineral lattices in

organic-poor sediments, U adsorbed on organic material in source rocks more readily releases ^{129}I from U fission to pore water[52,88]. As such, E_R/P_R is assumed to be 3 for sandstone reservoirs, whereas E_S/P_S is assumed to be 15 for source rocks. The value for t_{eq} is 90 Ma or any time prior.

Because both t_{MW} and ρ_S had two endmember values, the calculated t_S value of the evaporated seawater from each well varied within a certain range (Table S2, Fig. 9a). However, the results demonstrated that the evaporated seawater migrated into the reservoirs at different times. The evaporated seawater in DB304 and DB304-1 was the youngest ($t_{S\text{-}avg}$=5.70 and 12.41 Ma), whereas that in DB101-5 was the oldest ($t_{S\text{-}avg}$=68.97 Ma). The $t_{S\text{-}avg}$ values for the other four water bodies ranged from 22.73 to 36.31 Ma. Overall, the charging times for the evaporated seawater decreased eastward.

Figure 9. Calculated migration times of evaporated seawater (t_S), with a west-east-trending distribution (**a**), and the relationship between t_S and the dryness coefficient of natural gas (**b**) in the BD East District.

Different episodes of evaporated seawater and related gases in the DB East District

The different migration times of evaporated seawater in the DB East District could indicate different episodes of natural gas formation. All the gases were enriched in methane and thus exhibited high dryness coefficients (>97%, Table S4). However, the dryness coefficients differed among the wells. As shown in Fig. 9b, t_S and the dryness coefficient are negatively related. These findings indicate that the maturity of the gases that reached different wells varied. The first-charged gas was the least mature and thus had the lowest dryness coefficient (97.1% of DB102, 97.1% of DB101-5, and 97.3% of DB101-1), whereas the second-charged gases were derived from more mature source rocks and thus had relatively high dryness coefficients (97.7% of DB209 and 97.8% of DB202). The third-charged gases were characterized by the highest dryness coefficients (98.4% for DB304 and 98.7% for DB304-1). The distribution of $\delta^{13}C_{CH4,}$ which was reported in a previous study, also supported the different episodes of hydrocarbon gases. It is widely accepted that the late-charged gas with the highest maturity has the heaviest $\delta^{13}C_{CH4}$. Here, the $\delta^{13}C_{CH4}$ in the southeast of the DB East District had the heaviest value (-29.7‰, n=3), while it was lightest in the northeast (-30.6‰, n=5)[73]. The gases in the middle location have an intermediate value of $\delta^{13}C_{CH4}$ (-30.4‰, n=4)[73]. Furthermore, the migration times of

both the gases and the evaporated seawater were strongly related to the local activities of the thrust faults. In the DB East District, three thrust faults developed from northeast to southwest (Keshen No. 1 Fault, Keshen Fault, and Keshen No. 4 Fault; Fig. 1a and Fig. 10). These faults are considered to have formed via compression by the Tianshan Orogenic Belt since the Miocene and have experienced different developmental stages (e.g., sealing or reopening)[34,73]. It appears that the opening times of these faults followed the order of the Keshen No. 1 Fault, Keshen Fault, and Keshen No. 4 Fault. Therefore, the natural gas and associated evaporated seawater from the deep Triassic–Jurassic source rocks migrated along the trough faults into the reservoirs at different times.

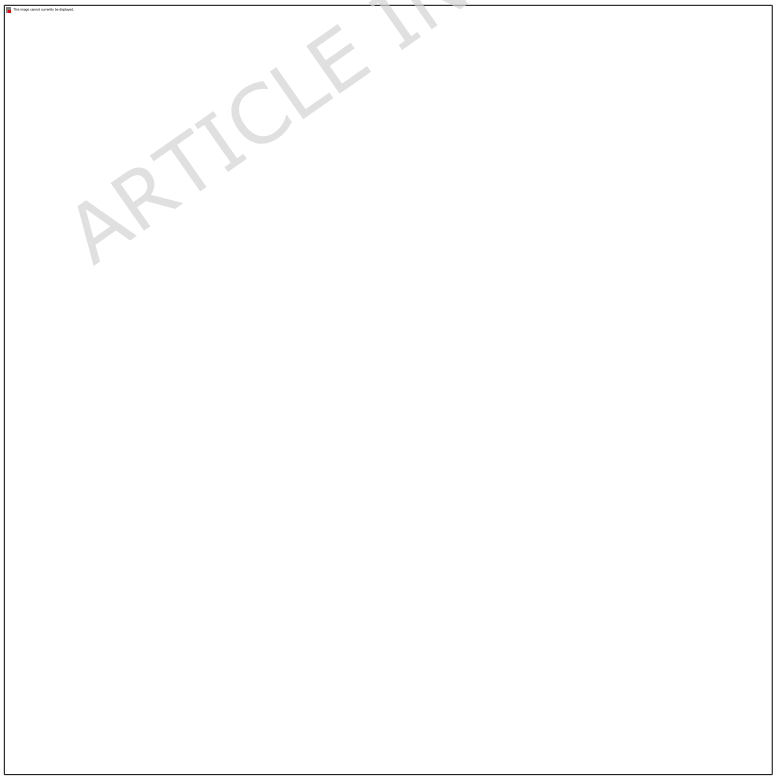

Figure 10. Comigration model of evaporated seawater and gases in the DB East District. The base map was modified from Zhang et al.[72]. The percentages shown in this figure are the dryness coefficients of the natural gases.

The calculated t_S values were not accurate. The t_S values were clearly greater than the charge times of the gases estimated from the inclusion analysis (3–2 Ma)[43,44] and the modeled gas generation times for the source rocks (<5 Ma)[34,36]. Furthermore, some t_S values occurred earlier than the formation time of the thrust fault system (Miocene, <23.3 Ma), which was associated with the main upward migration pathway of both hydrocarbons and evaporated seawater. The anomalously higher t_S values could be attributed to the low C_{129} value, which was due to the presence of residual water before the charging of the gas-related evaporated seawater and/or the addition of condensed water. Three kinds of residual water, including connate water when the reservoir sandstones were deposited, meteoric water during the denudation period in the Late Cretaceous and residual brine associated with early charged oils, were presumably displaced by later fluids. Under geological conditions, all three types of fluids were retained in the formation water to some degree and exhibited low C_{129} values as a result of the long-term delay in ^{129}I in the reservoirs. In addition, the dilution of condensed water during gas recovery reduced the C_{129} content. Therefore, both the presence of residual water and the dilution of condensed water decreased the C_{129} content and thus increased the calculated t_S value in the dating model

(Fig. S2). Nevertheless, the different gas accumulation periods among the wells in the DB East District were revealed by the t_S values of the evaporated seawater.

Geological implications

With petroleum exploration occurring in deep and ultradeep strata, many gas accumulations have been discovered worldwide[20]. However, unlike crude oils, natural gas is compositionally simple. It is typically composed of several kinds of low-molecular-weight organic (mainly C_1–C_5) and inorganic (e.g., CO_2 and N_2) gaseous compounds. As a product of kerogen maturation and/or oil cracking under high thermal stress, these gaseous compounds provide only limited geochemical information, such as the kerogen type, maturity stage, and gas–gas relationship[89]. The accumulation processes of natural gases are difficult to elucidate clearly from gas geochemistry. Given these factors, attention should be focused on the geochemistry of formation water.

The chemical and isotopic compositions of formation water can not only reveal the origins and evolution processes of the water but also constrain the sources and accumulation processes of the gas. This case study was a preliminary attempt at obtaining such information. However, several problems urgently need to be solved. First, the evolution process of pore water during the maturation of source rocks requires further investigation. Information such as the amount and occurrence state of pore water, relative proportions of pore water and hydrocarbons, and compositions of pore water is key to explaining the

coexpulsion behavior of both pore water and hydrocarbons; notably, this information can be used to develop a precise ^{129}I dating technique and new tracing indicators. Second, the dating technique should be further improved. Some of the parameters used in the dating equations (e.g., E and P) were assigned on the basis of the user's experience. The other parameters vary over large scales as a result of fluid mixing and other geological factors. More precise dating results could be obtained if these parameters are further constrained and several different dating methods (e.g., ^{129}I and ^{36}Cl) are used together. Finally, the influence of condensed water on produced water needs to be quantitatively assessed to obtain the true chemical and isotopic compositions of the formation water and fully utilize the water data. In summary, by combining the geochemistry of both natural gas and produced water, the overall and precise accumulation processes of natural gas, especially the differentiated accumulation processes in a given region, can be revealed.

Conclusions

In this study, we systemically analyzed the chemical and isotopic compositions of the water produced in a deep BD gas field in northwestern China. The main conclusions are as follows.

1. The formation water mainly consists of halite-dissolution meteoric water and low proportions of iodine-rich evaporated seawater. The former infiltrated the $E_{1\text{-}2}$km halite during the Kangcun–Kuqa stage (Middle Miocene to

Pliocene, 16.3–1.64 Ma). The latter migrated together with natural gas from some layers in the Triassic–Jurassic source rocks that were influenced by seawater invasion. In addition, connate water or other water (e.g., meteoric water during the denudation period of the Late Cretaceous) could have been retained to some degree.

2. Compared with the formation water, the condensed water had lower TDS contents, lower δD and δ^{18}O values, and different ionic compositions. Most of the produced water displayed characteristics of mixing between formation water and condensed water to different degrees.

3. On the basis of a dating model of ^{129}I in the formation water, different episodes of evaporated water and associated natural gas were observed among the wells in the DB East District, although the precise timing for the migration of evaporated seawater was difficult to determine.

Together, the results of this case study add to our understanding of the movement of hydrocarbon-related geological fluids in deep basins and suggest that the chemical and isotopic composition of formation water could be used together with that of gas to constrain the sources and accumulation processes of deeply buried gas.

Funding

This study was financially supported by the National Natural Science Foundation of China (grant nos. 42125304 and 42573026). Theory of hydrocarbon enrichment

under multisphere interactions of the Earth (THEMSIE04010104), and the State Key Laboratory of Organic Geochemistry (SKLOG2024-03).

References

1. Moldowan, J. M., Albrecht, P., & Philp, R. P. *Biological markers in sediments and petroleum* (Prentice Hall, 1992).

2. Peters, K. E., Walters, C. C. & Moldowan, J. M. *The Biomarker Guide: Biomarkers and isotopes in the environment and human history* (Cambridge University Press, 2005).

3. Wang, S. S., Chen, J., Jia, W. L. & Peng, P. A. Multiple isotopes (C-S-N-H) and bound biomarkers in asphaltenes: New constraints on the classification and genesis of reservoir bitumens from the northwestern Sichuan Basin, South China. *Org. Geochem.* **193**, 104807 (2024).

4. Liu, D. Y. et al. The control of reservoir types in Lunnan oilfield on characters of formation water (in Chinese with English abstract). *Acta. Petrol. Sin.* **33**, 367-371 (2012).

5. Kharaka, Y. K. & Hanor, J. S. Deep fluids in the continents: I. sedimentary basins, in *Treatise on geochemistry: surface and ground water, weathering, and soils* (ed. Drever, J. I.). 1-48 (Elsevier-Pergamon, 2003).

6. Worden, R. H. Halogen elements in sedimentary systems and their evolution during diagenesis in *The Role of Halogens in Terrestrial and Extraterrestrial Geochemical Processes: Surface, Crust, and Mantle* (eds. Harlov, D. E. & Aranovich, L.) 185-260 (Springer International Publishing, 2018).

7. Fehn, U. Tracing crustal fluids: Applications of natural ^{129}I and ^{36}Cl. *Annu. Rev. Earth. Pl. Sc*. **40**, 45-67 (2012).

8. Franks, S. G. et al. Carbon isotopic composition of organic acids in oil field waters, San Joaquin Basin, California, USA. *Geochim. Cosmochim. Ac.* **65**, 1301-1310 (2001).

9. Mearns, E. W. & McBride, J. J. Hydrocarbon filling history and reservoir continuity of oil fields evaluated using ^{87}Sr/^{86}Sr isotope ratio variations in formation water, with examples from the North Sea. *Petrol. Geosci*. **5**, 17-27 (1999).

10. Bachu, S. Flow of formation waters, aquifer characteristics, and their relation to hydrocarbon accumulations, northern Alberta basin. *AAPG. Bull*. **81**, 712-733 (1997).

11. Sun, Z. Y., Chen, J., Wang, Q., Jia, W. L. & Peng, P. A. A quantitative analysis on thermochemical sulfate reduction products of two model compounds: Implications for reaction mechanism and alteration process of hydrocarbons. *Chem. Geol*. **661**, 122187 (2024).

12. Lewan, M. D. Experiments on the role of water in petroleum formation. *Geochim. Cosmochim. Ac*. **61**, 3691-3723 (1997).

13. Lewan, M. D. & Fisher, J. B. Chapter 4 Organic acids from petroleum source rocks in *Organic Acids in Geological Processes* (ed. Pittman, E. D.). 70-114 (Springer-Verlag, 1994).

14. Williams, L. B., Elliott, W .C. & Hervig, R. L. Tracing hydrocarbons in gas shale using lithium and boron isotopes: Denver Basin USA, Wattenberg Gas Field. *Chem. Geol*. **417**, 404-413 (2015).

15. Fabryka-Martin, J., Bentley, H., Elmore, D. & Airey, P. L. Natural iodine-129 as an environmental tracer. *Geochim. Cosmochim. Ac*. **49**, 337-347 (1985).

16. Moran, J. E., Fehn, U. & Hanor, J. S. Determination of source ages and migration patterns of brines from the U.S. Gulf Coast basin using ^{129}I. *Geochim. Cosmochim. Ac*. **59**, 5055-5069 (1995).

17. Birkle, P. Application of ^{129}I/^{127}I to define the source of hydrocarbons of the Pol-Chuc, Abkatún and Taratunich–Batab oil reservoirs, Bay of Campeche, southern Mexico. *J. Geochem. Explor*. **89**, 15-18 (2006).

18. Fehn, U., Snyder, G. & Egeberg, P. K. Dating of pore waters with ^{129}I: Relevance for the origin of marine gas hydrates. *Science*. **289**, 2332-2335 (2000).

19. Fehn, U., Snyder, G. T. & Muramatsu, Y. Iodine as a tracer of organic material: 129I results from gas hydrate systems and fore arc fluids. *J. Geochem. Explor*. **95**, 66-80 (2007).

20. Hao, F. & Liu, K. Introduction for the special issue on deep petroleum systems. *AAPG. Bull.* **108**, 1189-1191 (2024).

21. Peng, P. A. & Jia, C. Z. Evolution of deep source rock and resource potential of primary light oil and condensate (in Chinese with English abstract). *Acta. Petrol. Sin.* **42**, 1543-1555 (2021).

22. Andrew, A. S., Whitford, D. J., Berry, M. D., Barclay, S. A. & Giblin, A. M. Origin of salinity in produced waters from the Palm Valley gas field, Northern Territory, Australia. *Appl. Geochem*. **20**, 727-747 (2005).

23. Bagheri, R. et al. Hydrochemical and isotopic ($\delta^{18}O$, $\delta^{2}H$, $^{87}Sr/^{86}Sr$, $\delta^{37}Cl$ and $\delta^{81}Br$) evidence for the origin of saline formation water in a gas reservoir. *Chem. Geol*. **384**, 62-75 (2014).

24. Kharaka, Y. K., Callender, E. & Wallace, R. H. Geochemistry of geopressured geothermal waters from Frio Clay in Gulf Coast Region of Texas. *Geology*. **5**, 241-244 (1977).

25. Lei, G. L., Wang, X., Wu, C., Li, Q. & Xu, Z. P. *Tectonic characteristics and deformation mechanism of salt-related structures in Kuqa Depression, Tarim Basin (in Chinese)* (Petroleum Industry Press, 2014).

26. Yu, Y. X. et al. Salt structures and hydrocarbon accumulations in the Tarim Basin, northwest China. *AAPG. Bull*. **98**, 135-159 (2014).

27. Tang, L. J. et al. Salt-related structural styles of Kuqa foreland fold belt, northern Tarim basin. *Sci. China. Ser. D*. **47**, 886-895 (2004).

28. Wang, Z. M., Li, Y., Xie, H. W. & Neng, Y. Geological understanding on the formation of large-scale ultra-deep oil-gas field in Kuqa foreland basin (in Chinese with English abstract). *China. Petrol. Explor*. **21**, 37-43 (2016).

29. Lu, H. F. et al. Rejuvenation of the Kuqa Foreland Basin, Northern Flank of the Tarim Basin, Northwest China. *Int. Geol. Rev*. **36**, 1151-1158 (1994).

30. Jia, C. Z. & Wei, G. Q. Structural characteristics and petroliferous features of Tarim Basin. *Chinese. Sci. Bull*. **47**, 1-11 (2002).

31. Li, Z., Song, W. J., Peng, S. T., Wang, D. X. & Zhang, Z. P. Mesozoic-Cenozoic tectonic relationships between the Kuqa subbasin and Tian Shan, northwest China: constraints from depositional records. *Sediment. Geol*. **172**, 223-249 (2004).

32. Chen, S., Tang, L., Jin, Z., Jia, C. & Pi, X. Thrust and fold tectonics and the role of evaporites in deformation in the Western Kuqa Foreland of Tarim Basin, Northwest China. *Mar. Petrol. Geol*. **21**, 1027-1042 (2004).

33. Mo, T. et al. The phase characteristics and controlling factors of oil and gas in the west of Kelasu structural belt in Kuqa Depression, Tarim Basin (in Chinese with English abstract). *Nat. Gas. Geosci*. **35**, 1532-1543 (2024).

34. Zhao, M. J. & Lu, S. F. Two periods of reservoir forming and their significance for hydrocarbon distribution in Kuqa Depression (in Chinese with English abstract). *Acta. Petrol. Sin*. **24**, 16-25 (2003).

35. Jia, C., Gu, J. & Zhang, G. Geological constraints of giant and medium-sized gas fields in Kuqa Depression. *Chinese. Sci. Bull*. **47**, 47-54 (2002).

36. Zhao, W. et al. Gas systems in the Kuche Depression of the Tarim Basin: Source rock distributions, generation kinetics and gas accumulation history. *Org. Geochem*. **36**, 1583-1601 (2005).

37. Qin, S. F. & Dai, J. X. Distribution fo coal-derived oil and gas in Kuqa Depression and its control factors (in Chinese with English abstract). *Nat. Gas. Ind*. **26**, 16-18 (2006).

38. Lai, J. et al. Deep burial diagenesis and reservoir quality evolution of high-temperature, high-pressure sandstones: Examples from Lower Cretaceous Bashijiqike Formation in Keshen area, Kuqa depression, Tarim basin of China. *AAPG Bull*. **101**, 829-862 (2017).

39. Zeng, Q. et al. Characteristics, genetic mechanism and oil & gas exploration significance of high-quality sandstone reservoirs deeper than 7000 m: A case study of the Bashijiqike Formation of Lower Cretaceous in the Kuqa Depression, NW China. *Nat. Gas. Ind. B*. **7**, 317-327 (2020).

40. Zhang, H. et al. Characterization and evaluation of ultra-deep fracture-pore tight sandstone reservoirs: A case study of Cretaceous Bashijiqike Formation in Kelasu tectonic zone in Kuqa foreland basin, Tarim, NW China. *Petrol. Explor. Dev*. **41**, 175-184 (2014).

41. Wang, X. et al. Cenozoic paleo-environmental evolution of the Pamir–Tien Shan convergence zone. *J. Asian. Earth. Sci*. **80**, 84-100 (2014).

42. Wei, L. Y. et al. Reconstruction of the proto-type basin and tectono-paleographical evolution of Tarim in the Cenozoic. *Front. Earth. Sci*. **11**, 1095002 (2023).

43. Guo, X. W. et al. Fluid evolution in the Dabei Gas Field of the Kuqa Depression, Tarim Basin, NW China: Implications for fault-related fluid flow. *Mar. Petrol. Geol*. **78**, 1-16 (2016).

44. Guo, X. W. et al. Hydrocarbon accumulation processes in the Dabei tight-gas reservoirs, Kuqa Subbasin, Tarim Basin, northwest China. *AAPG. Bull*. **100**, 1501-1521 (2016).

45. Zhao, S. F., Chen, W., Zhou, L., Zhou, P. & Zhang, J. Characteristics of fluid inclusions and implications for the timing of hydrocarbon accumulation in the cretaceous reservoirs, Kelasu Thrust Belt, Tarim Basin, China. *Mar. Petrol. Geol*. **99**, 473-487 (2019).

46. Clescerl, L. S., Greenberg, A. E. & Eaton, A. D. *Standard methods for the examination of water and wastewater, 20th ed*. (American Public Health Association, 1999).

47. Chen, N., Hou, X., Zhou, W., Fan, Y. & Liu, Q. Analysis of low-level ^{129}I in brine using accelerator mass spectrometry. *J. Radioanal. Nucl. Ch*. **299**, 1965-1971 (2014).

48. Zhou, W. et al. Analysis and environmental application of ^{129}I at the Xi'an Accelerator Mass Spectrometry Center. *Nucl. Instrum. Meth. B*. **294**, 147-151 (2013).

49. Zhou, W. J. & Hou, X. L. Preliminary study of radioisotope ^{129}I application in China using Xi'an Accelerator Mass Spetrometer. *INCS. News*. **7**, 9-23 (2010).

50. Davis, S. N. The chemistry of saline waters: discussion. *Ground. Water*. **2**, 51-51 (1964).

51. Chen, J. et al. The sources and formation processes of brines from the Lunnan Ordovician paleokarst reservoir, Tarim Basin, northwest China. *Geofluids*. **13**, 381-394 (2013).

52. Chen, J. et al. Origin and evolution of oilfield waters in the Tazhong oilfield, Tarim Basin, China, and their relationship to multiple hydrocarbon charging events. *Mar. Petrol. Geol*. **98**, 554-568 (2018).

53. Huang, T. M. & Pang, Z. H. Changes in groundwater induced by water diversion in the Lower Tarim River, Xinjiang Uygur, NW China: Evidence from environmental isotopes and water chemistry. *J. Hydrol*. **387**, 188-201 (2010).

54. Shan, J. J. et al. Origin and circulation of saline springs in the Kuqa Basin of the Tarim Basin, Northwest China. *J. Arid. Land*. **12**, 331-348 (2020).

55. Li, F. H. & Yan, W. S. *Principles of hydrogeology of oil and gas fields (in Chinese)* (Petroleum Industry Press, 1991).

56. Lico, M. S., Kharaka, Y. K., Carothers, W. W. & Wright, V. A. *Methods for collection and analysis of geopressured geothermal and oil field waters, USGS-WSP-2194* (Geological Survey, 1982).

57. Molofsky, L. J. et al. Evidence for water of condensation: A third source of water in shale gas wells. *AAPG. Bull*. **107**, 629-641 (2023).

58. Horita, J. & Wesolowski, D. J. Liquid-vapor fractionation of oxygen and hydrogen isotopes of water from the freezing to the critical-temperature. *Geochim. Cosmochim. Ac*. **58**, 3425-3437 (1994).

59. McCaffrey, M. A., Lazar, B. & Holland, H. D. The evaporation path of seawater and the coprecipitation of Br^- and K^+ with halite. *J. Sediment. Res*. **57**, 928-937 (1987).

60. Kloppmann, W. et al. Halite dissolution derived brines in the vicinity of a Permian salt dome (N German Basin).: Evidence from boron, strontium, oxygen, and hydrogen isotopes. *Geochim. Cosmochim. Ac*. **65**, 4087-4101 (2001).

61. Pinti, D. L. et al. Fossil brines preserved in the St-Lawrence Lowlands, Québec, Canada as revealed by their chemistry and noble gas isotopes. *Geochim. Cosmochim. Ac*. 75, 4228-4243 (2011).

62. Worden, R. H., Manning, D. A. C. & Bottrell, S. H. Multiple generations of high salinity formation water in the Triassic Sherwood Sandstone: Wytch Farm oilfield, onshore UK. *Appl. Geochem*. **21**, 455-475 (2006).

63. Fontes, J. C. & Matray, J. M. Geochemistry and origin of formation brines from the Paris Basin, France .1. brines associated with Triassic salts. *Chem. Geol*. **109**, 149-175 (1993).

64. Zherebtsova, I. K. & Volkova, N. N. Experimental study of behavior of trace elements in the process of natural solar evaporation of Black Sea water and Sasyk-Sivash brine. *Geochem. Int*. **3**, 656-670 (1966).

65. Engle, M. A. et al. Geochemistry of formation waters from the Wolfcamp and "Cline" shales: Insights into brine origin, reservoir connectivity, and fluid flow in the Permian Basin, USA. *Chem. Geol*. **425**, 76-92 (2016).

66. Ellrich, J., Hirner, A. & Stärk, H. Distribution of trace elements in crude oils from southern Germany. *Chem. Geol*. **48**, 313-323 (1985).

67. Moran, J. E., Teng, R. T. D., Rao, U. & Fehn, U. Detection of iodide in geologic materials by high-performance liquid chromatography. *J. Chromatogr. A*. **706**, 215-220 (1995).

68. Fehn, U., Tullai, S., Teng, R. T. D., Elmore, D. & Kubik, P. W. Determination of 129I in heavy residues of two crude oils. *Nucl. Instrum. Meth. B*. **29**, 380-382 (1987).

69. Muramatsu, Y. & Wedepohl, K.H. The distribution of iodine in the Earth's crust. *Chem. Geol*. **147**, 201-216 (1998).

70. Liang, D. G. et al. *The generation of terresital oil and gas in Kuqa Depression, Tarim Basin (in Chinese)* (Petroleum Industry Press, 2004).

71. Zhang, B. M., Chen, J. P., Bian, L. Z. & Zhang, S. C. Rediscussion on the Sea-slooding events during Triassic to Jurassic of Kuqa Depression in Tarim Basin (in Chinese with Engligh abstract). *Acta. Geol. Sin*. **80**, 236-244 (2006).

72. Zhang, S. C., Zhang, B., Zhu, G. Y., Wang, H. T. & Li, Z. X. Geochemical evidence for coal-derived hydrocarbons and their charge history in the Dabei Gas Field, Kuqa Thrust Belt, Tarim Basin, NW China. *Mar. Petrol. Geol*. **28**, 1364-1375 (2011).

73. Wei, Q. et al. Hydrocarbon geochemistry and charging history of the deep tight sandstone reservoirs in the Dabei Gas Field, Kuqa Depression, Tarim Basin, NW China. *Enger. Explor. Exploit*. **38**, 2325-2355 (2020).

74. Deng, H. Y. et al. Genetic identification of light oils and condensates using δD indices of C_7 hydrocarbons: A case study in the Tarim Basin, NW China. *Int. J. Coal. Geol*. **279**, 104372 (2023).

75. Boyer, C., Kieschnick, J., Suarez-Rivera, R., Lewis, R. E. & Walters, G. Producing gas from its source. *Oilfield. Rev.* **18**, 36-49 (2006).

76. Cipolla, C. L., Lolon, E. P., Erdle, J. C. & Rubin, B. Reservoir modeling in shale-gas reservoirs. *Int. Petrol. Tech. Conf.* 13185 (2009).

77. Cheng, P. et al. Differences in the distribution and occurrence phases of pore water in various nanopores of marine-terrestrial transitional shales in the Yanquan area of the northeast Qinshui Basin, China. *Mar. Petrol. Geol*. **137**, 10510 (2022).

78. Cheng, P., Xiao, X. M., Wang, X., Sun, J. & Wei, Q. Evolution of water content in organic-rich shales with increasing maturity and its controlling factors: Implications from a pyrolysis experiment on a water-saturated shale core sample. *Mar. Petrol. Geol*. **109**, 291-303 (2019).

79. Morton, R. A. & Land, L. S. Regional variations in formation water chemistry, Frio Formation (Oligocene), Texas Gulf Coast. *AAPG. Bull.* **71**, 191-206 (1987).

80. Xie, X. N., Jiu, J. J., Li, S. T. & Cheng, J. M. Salinity variation of formation water and diagenesis reaction in abnormal pressure environments. *Sci. China. Ser. D*. **46**, 269-284 (2003).

81. Fehn, U., Moran, J. E., Snyder, G. T. & Muramatsu, Y. The initial ^{129}I/I ratio and the presence of 'old' iodine in continental margins. *Nucl. Instrum. Meth. B*. **259**, 496-502 (2007).

82. Fabryka-Martin, J. T., Davis, S. N., Elmore, D. & Kubik, P. W. In situ production and migration of ^{129}I in the Stripa granite, Sweden. *Geochim. Cosmochim. Ac*. **53**, 1817-1823 (1989).

83. Chen, J. et al. Iodine-129 chronological study of brines from an Ordovician paleokarst reservoir in the Lunnan oilfield, Tarim Basin. *Appl. Geochem*. **65**, 14-21 (2016).

84. Zhang, L. et al. Level and source of ^{129}I of environmental samples in Xi'an region, China. *Sci. Total. Environ*. **409**, 3780-3788 (2011).

85. Zhao, G. L. Petrology and geochemistry of sediments from Cretaceous-Tertiary in the Tarim Basin (in Chinese with English abstract). *J. Miner. Petrol*. **32**, 81-93 (2012).

86. Liang, D. G., Zhang, S. C., Chen, J. P., Wang, F. Y. & Wang, P. R. Organic geochemistry of oil and gas in the Kuqa depression, Tarim Basin, NW China. *Org. Geochem*. **34**, 873-888 (2003).

87. Thomas, L. *Coal Geology, 2nd* (John Wiley & Sons, Ltd, 2013).

88. Moran, J. E. Origin of iodine in the Anadarko Basin, Oklahoma: An ^{129}I study. *AAPG. Bull*. **80**, 658-694 (1996).

89. Peng, P. A. et al. Identification indexes and diagrams for natural gas origin: Connotation, significance and application. *Petrol. Explor. Dev*. **52**, 573-586 (2025).

Acknowledgements

We are grateful to Chen Naidong, Chen Chengshen, and Wang Jingchen for their assistance with sample collection and chemical analysis.

Author contributions

J.C. wrote the main manuscript text. Y.F., N.C. and J.X. conducted the experimental work. J.C. and Y.F. analyzed the results. H.Z. and T.M. provided the geological information of Bozi-Dabei gas field. W.J. and Y.W. improved the paper's structure and language. H.Z., T.M., X.H. and P.P. revised the manuscript. All authors reviewed the manuscript.

Additional information

Competing interests

The authors declare no competing interests.

Data Availability Statement

All data generated or analyzed during this study are included in this published article and its Supplementary Information files.